AJNR

Altered Functional Connectivity and Amyloid Deposition in PTSD-Associated Cognitive Impairment

Richard Dagher, Parisa Arjmand, Daniel A. Stevens, Max Wintermark, Haris I. Sair, Vivek Yedavalli and Licia P. Luna

Altered Functional Connectivity and Amyloid Deposition in PTSD-Associated Cognitive Impairment

Richard Dagher, Parisa Arjmand, Daniel A. Stevens, Max Wintermark, Haris I. Sair, Vivek Yedavalli, Licia P. Luna; for the Alzheimer's Disease Neuroimaging Initiative*

ABSTRACT

BACKGROUND AND PURPOSE: PTSD has been linked to an increased risk of cognitive impairment and dementia, with neuroinflammation, metabolic dysfunction, and neuropathological markers such as beta-amyloid and tau implicated as potential mechanisms. However, the roles of altered functional connectivity and amyloid deposition as biomarkers in the progression of cognitive impairment among PTSD patients remain unclear, with limited and often conflicting evidence from existing neuroimaging studies. This study examines these neuroimaging markers in PTSD patients with and without cognitive impairment to better understand the neurobiological pathways contributing to cognitive decline in PTSD.

MATERIALS AND METHODS: Data were obtained from the Alzheimer's Disease Neuroimaging Initiative (ADNI) and Department of Defense (DOD) ADNI databases. A cohort of 178 age-matched male subjects was divided into four groups: PTSD with cognitive impairment (CI) (PTSD-CI); PTSD and cognitively normal (CN) (PTSD-CN); non-PTSD (NPTSD with CI (NPTSD-CI); and NPTSD and CN (NPTSD-CN). All subjects underwent resting-state functional MRI and amyloid PET imaging, with PTSD diagnosis and CI confirmed through clinical assessments. Functional connectivity was analyzed using the CONN Toolbox, and amyloid burden was quantified via standardized uptake value ratios. Analyses controlled for demographic and genetic factors, including age, education, APOE4 status, and depression.

RESULTS: Compared to the NPTSD-CN group, the PTSD-CI group showed significantly increased amyloid uptake in the temporal and parietal lobes, with corresponding functional connectivity increase between the bilateral temporal lobes and parietal operculum. In contrast, PTSD-CN patients exhibited no significant amyloid increase but showed increased connectivity between the salience network, postcentral gyri and sensorimotor areas, and decreased connectivity between the sensorimotor network and anterior cingulate cortex. These distinct patterns suggest differing neurobiological profiles between PTSD-CI and PTSD-CN patients.

CONCLUSIONS: The findings suggest that elevated amyloid and altered connectivity patterns are associated with CI in PTSD, particularly in the temporal and parietal regions. In contrast, PTSD without cognitive decline was associated with functional connectivity changes in salience and sensorimotor networks but no increased amyloid deposition. This study underscores the importance of neuroimaging biomarkers in understanding PTSD-related cognitive decline and suggests avenues for further investigation into the mechanistic pathways involved.

ABBREVIATIONS: ACC = anterior division of the cingulate gyrus; ADAS-Cog = Alzheimer's Disease Assessment Scale-Cognitive; CAPS = Clinician-Administered PTSD Scale; PTSD = post-traumatic stress disorder; CI = cognitively impaired; CN = cognitively normal; ECog = Everyday Cognition; GDS = Geriatric Depression Scale; MoCA = Montreal Cognitive Assessment; NPTSD = non-PTSD.

SUMMARY SECTION

PREVIOUS LITERATURE: PTSD has been identified as a significant risk factor for cognitive impairment and dementia, suggesting involvement of neuroinflammation, metabolic dysfunction, and neuropathological markers like beta-amyloid. Resting-state functional MRI (rs-fMRI) and amyloid PET imaging have shown promise in elucidating the neurobiological mechanisms underlying PTSD-associated cognitive decline. However, findings remain inconsistent, partly due to variations in study design and limited focus on PTSD with cognitive impairment (PTSD-CI). Structural and functional imaging studies highlight altered connectivity in default mode and salience networks, with amyloid deposition linked to functional changes. Existing research underscores the need to integrate multimodal imaging for deeper insights into PTSD-related neurodegeneration.

KEY FINDINGS: PTSD-CI subjects demonstrated increased amyloid uptake in temporal and parietal lobes and altered connectivity between temporal and parietal regions. PTSD subjects without cognitive decline (PTSD-CN) showed functional connectivity changes without increased amyloid deposition. Overlapping regions of abnormal connectivity and amyloid burden suggest distinct neurobiological profiles between PTSD-CI and PTSD-CN patients.

KNOWLEDGE ADVANCEMENT: This study highlights the utility of integrating rs-fMRI and amyloid PET imaging in understanding PTSD-related cognitive decline. The observed connectivity changes may represent compensatory mechanisms in response to amyloid deposition. These findings advance our understanding of PTSD-associated neurodegeneration, offering potential pathways for early diagnosis and targeted therapeutic interventions.

INTRODUCTION

Growing evidence suggests that post-traumatic stress disorder (PTSD) may increase the risk of mild cognitive impairment and dementia.[1-3] Studies indicate that individuals with PTSD are twice as likely to develop dementia compared to those without the disorder,[3] and a recent meta-analysis further confirmed that PTSD is a significant risk factor for all-cause dementia.[4] Although the exact mechanisms linking PTSD to cognitive impairment (CI) remain unclear, several biological pathways have been proposed, including neuroinflammation, metabolic dysfunction, and neuropathological markers such as beta-amyloid and tau.[1,5-7]

Neuroimaging studies examining the relationship between PTSD and CI are sparse and often yield inconsistent findings. Many fail to adequately control for confounding factors such as age, race, education, and co-occurring disorders like major depression and anxiety.[8] A recent systematic review highlighted structural and metabolic abnormalities in the brain, particularly temporal and parietal lobes, akin to those seen in dementia, as observed through FDG-PET and structural MRI in individuals with PTSD and cognitive decline.[8] However, to our knowledge, no resting-state fMRI studies have specifically explored this association. Unlike structural imaging, resting-state fMRI can reveal alterations in brain activity and connectivity that may precede observable structural changes, offering early insights into the progression of cognitive decline.[9] Additionally, resting-state fMRI allows for the investigation of network-level dysfunctions, such as those in the default mode network, which are often implicated in both PTSD and dementia.[10]

While other MRI techniques, such as DTI, are well-suited for assessing structural connectivity, resting-state fMRI offers unique insights into functional connectivity patterns. There is growing evidence that resting-state fMRI parameters can differentiate between amyloid-positive and negative individuals, even in the early stages of cognitive decline.[11] For instance, studies using resting-state fMRI have consistently found decreased functional connectivity in the default mode network of individuals with elevated brain amyloid, even in cognitively normal elderly adults.[12-14] Moreover, it has been proposed that the initial buildup of Aβ fibrils is linked to increased functional connectivity, occurring before any structural changes.[15,16] Given these capabilities, resting-state fMRI, in combination with amyloid PET imaging, provides a complementary understanding of brain function and pathology in PTSD. This combined approach could help elucidate the complex interplay between amyloid burden and connectivity disruptions.

Because depressive symptoms are associated with functional MRI abnormalities and altered amyloid uptake, it is crucial to control for depression when analyzing PTSD data.[17-19] Additionally, several studies combine datasets of individuals with both PTSD and traumatic brain injury, which complicates interpretation, as traumatic brain injury independently contributes to metabolic and functional abnormalities, making it difficult to disentangle its effects from those of PTSD.[20-22] Research on amyloid uptake in PTSD veterans also presents mixed findings, with reports of both increased and decreased amyloid concentrations in male veterans, although cognitive impairment and depression scores were not directly considered in these analyses.[23,24] Several other lifestyle factors, like alcohol and tobacco, have been also found to be linked to cognitive decline.[25]

Given these challenges, our study aims to re-examine the relationship between PTSD and cognitive decline, focusing on amyloid and functional MRI data in PTSD patients without traumatic brain injury while controlling for depression. We hypothesized that PTSD patients with cognitive impairment would display distinct patterns of functional connectivity and amyloid distribution compared to those without cognitive decline. Additionally, we suggest that the observed changes in functional connectivity may reflect compensatory mechanisms responding to amyloid deposition, which is associated with cognitive impairment.

MATERIALS AND METHODS

Study Subjects

Data from PTSD subjects were obtained from the Alzheimer's Disease Neuroimaging Initiative - Department of Defense (ADNI-DOD) database, a multimodal (MRI, PET, and neuropsychological assessment), nonrandomized study that recruited Vietnam War veterans from the Department of Veterans Affairs, investigating PTSD or traumatic brain injury as potential risk factors for the development of AD. Data from subjects without PTSD (cognitively normal [CN] and cognitively impaired [CI] controls) were also obtained from the ADNI database, which was launched in 2003 as a public-private partnership led by Principal Investigator Michael W. Weiner, MD. The primary goal of ADNI has been to test whether serial MRI, PET, other biological markers, and clinical and neuropsychological assessment can be combined to measure the progression of mild cognitive impairment and AD. For up-to-date information, see https://adni.loni.usc.edu.

Age-matched male subjects were classified into four groups: CI and CN controls (non-PTSD [NPTSD]-CI and NPTSD-CN) and PTSD groups (PTSD-CI and PTSD-CN). Assessments included T1-weighted structural MRI, resting-state fMRI, cognitive testing, and genetic analysis. A total of 178 subjects underwent a resting-state fMRI and an amyloid PET imaging. Of those, 60 patients met clinical criteria for PTSD, while 118 subjects were included in control groups (55 NPTSD-CI, 63 NPTSD-CN). All NPTSD-CN subjects had an amyloid-negative scan (see Supplementary Material).

Neuropsychological Assessment

All participants underwent a battery of cognitive and neuropsychological assessments, including the Montreal Cognitive Assessment (MoCA), Everyday Cognition (ECog), Mini-Mental State Exam, Alzheimer's Disease Assessment Scale-Cognitive (ADAS-Cog), Clinical Dementia Rating, and Geriatric Depression Scale (GDS). MoCA was the primary neuropsychological test used to categorize PTSD patients into CI and control subgroups. A clinical cutoff score 26 is recommended to detect mild CI in elders.[26] We used the Clinician-Administered PTSD Scale (CAPS - lifetime, DSM-IV version) to assess for PTSD. A score of 40 or higher (lifetime) constituted the inclusion criteria for the PTSD group. As previously described, a CAPS score of 30 or below formed the inclusion criteria for control groups.[27] Subjects who scored between 30 and 40 were excluded based on the presumption that they had fluctuating and sub-threshold symptoms.[27] Patients with a MOCA > 26, Mini-Mental State Exam > 27, and Clinical Dementia Rating = 0 were classified as CN. Otherwise, they were classified as CI. To isolate the effects of PTSD, we excluded any patients with a documented history of traumatic brain injury. Age-matched CI controls were selected based on similar MoCA scores, and only subjects with MoCA scores between 18 and 26 were included to indicate CI[28] (See Figure 1).

Resting-state functional MRI

Resting-state fMRI data acquisition

All imaging data were acquired on 3T scanners at rigorously validated sites with a standardized protocol,[29] including sagittal MPRAGE and resting-state fMRI. Functional and structural MRI protocol details are available at https://adni.loni.usc.edu/data-samples/adni-data/neuroimaging/mri/ and https://adni.loni.usc.edu/wp-content/uploads/2017/09/DODADNI_Procedures_Manual_20170912.pdf.

Resting-state fMRI data preprocessing

Resting-state fMRI data were preprocessed and analyzed using the default pipeline in CONN Functional Connectivity Toolbox (RRID:SCR_009550 release 22; https://web.conn-toolbox.org/)[30,31] and the statistical parametric mapping software (SPM12).[32,33] Resting-state fMRI preprocessing steps are detailed in the Supplementary Material.

ROI-to-ROI connectivity whole brain analysis

ROI-to-ROI connectivity matrices were generated, using Pearson correlation to quantify functional connectivity patterns in 164 HPC-ICA networks[31] and Harvard-Oxford atlas ROIs.[34] Connections were thresholded at an uncorrected $p < 0.05$ after a cluster-level FDR correction at $p < 0.05$, and then sorted using hierarchical clustering. When no significant results were observed using cluster-level inferences, parametric multivariate ROI-based inferences were applied (cluster threshold: $p < 0.05$, ROI-level FDR corrected; connection threshold: uncorrected $p < 0.01$). Age, education, APOE4 status, and GDS scores were included as covariates in group-level ROI-to-ROI connectivity GLM analyses when comparing PTSD and NTPSD groups.

Florbetapir (AV-45) PET imaging

PET acquisition

Amyloid PET images were acquired using Florbetapir across various scanners. Data were obtained through a 30-minute, six-frame dynamic scan or a static 30-minute single-frame scan, both performed 30 to 60 minutes post-injection (details are available at https://adni.loni.usc.edu/data-samples/adni-data/neuroimaging/pet/ and https://adni.loni.usc.edu/wp-content/uploads/2017/09/DODADNI_Procedures_Manual_20170912.pdf).

PET data preprocessing

PET data were processed using SPM12 and FMRIB's Software Library[35] (FSL 5.0.9, Analysis Group, FMRIB, Oxford, UK, 2012).[32,33] PET preprocessing steps are detailed in the Supplementary Material.

Single-Subject and Group-Level Florbetapir PET SPM Analyses

Whole-brain 2-sample t-test analysis was performed at the voxel level using SPM12 software to compare PTSD-CI, PTSD-CN, and NPTSD-CI with NPTSD-CN elderly controls and identify clusters of increased tracer uptake between groups. A GLM of the preprocessed PET data was constructed, treating all subjects from all subgroups as one combined group to allow for direct statistical comparisons between subgroups. Age, education status, APOE4 status, and GDS scores were individually introduced as variables of no interest in separate univariate GLMs to control for their potential confounding effects on tracer uptake. Statistical analysis was conducted using two thresholding approaches. We first applied cluster-level family-wise error (FWE) correction at $p < 0.05$. However, given the exploratory nature of this analysis, we also utilized a more liberal uncorrected threshold of $p < 0.001$, which facilitated better visualization of the overall pattern of amyloid uptake, particularly in regions with early or less pronounced accumulation.[36]

Other statistical analyses

Demographic and clinical characteristics between PTSD patients and controls were compared using MATLAB (MathWorks, R2023b). One-way ANOVA was used to evaluate differences in continuous variables, followed by post hoc multiple comparisons (using the multcompare function). Categorical variables were assessed with a chi-square test. Statistical significance was set at $p < 0.05$. Overlap between the resting-state fMRI regions of interest and the amyloid PET thresholded maps was calculated using Dice-Sørensen coefficient[37].
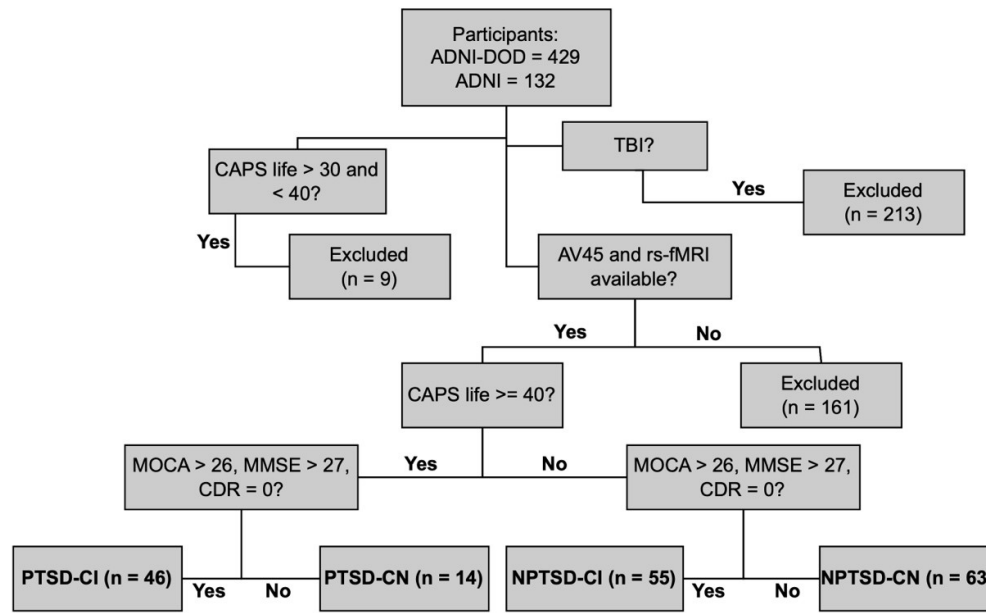
FIG 1. Subject selection flow chart.

RESULTS

Demographic and clinical characteristics

PTSD-CI, PTSD-CN, NPTSD-CI, and NPTSD-CN groups included 46, 14, 55, and 63 subjects, respectively. Table 1 summarizes their demographic and clinical characteristics. PTSD patients demonstrated a statistically significant lower educational attainment compared to NPTSD subjects, with averaging of 14.4 and 14.7 years versus 16.6 and 16.8 years for NPTSD subjects. Differences in ethnic composition were significant among groups. The PTSD-CI cohort had a higher percentage of Hispanic/Latino individuals (15.2%) compared to the NPTSD-CN group (3.2%). Additionally, there were notable differences in racial demographics, with higher numbers of African American and mixed-race individuals in the PTSD-CI group compared to the NPTSD-CI group. Significant differences were observed in clinical assessments (CAPS, MoCA, ADAS-Cog, Ecog total, and Clinical Dementia Rating) between PTSD-CI and NPTSD-CN groups. GDS total scores also differed between PTSD and non-PTSD subjects. While the frequency of APOE ε4 allele carriers did not significantly differ between the NPTSD-CN group (22.2%) and PTSD subjects, a significant difference was noted between PTSD groups (21.7% and 21.4%) and NPTSD-CI (38.2%).

Group differences in whole-brain ROI-to-ROI resting-state fMRI imaging analyses

PTSD-CI vs NPTSD-CN

A cluster of 11 regions of interest (ROIs) and 12 connections was identified (Figure 2A, Supplementary Table S1), with significant increased connectivity between the bilateral inferior temporal gyrus (temporooccipital part, toITG), bilateral superior temporal gyrus (STG), planum temporale (PT), parietal operculum (PO), and the right insular cortex (IC).

PTSD-CN vs NPTSD-CN

Nine statistically significant connectivity changes were found (4 positive correlations and 5 negative correlations) (Table S2 and Figure 2B). The increased connections were between the salience network in the rostral prefrontal cortex, left and right postcentral gyrus, and superior and right lateral sensorimotor network. The decreased connections observed were between the bilateral lateral sensorimotor network and anterior division of the cingulate gyrus (ACC), the salience network in the ACC, and between the bilateral precentral gyri and ACC.

PTSD-CI vs PTSD-CN and PTSD-CI vs NPTSD-CI

The results for these comparisons can be found in the Supplementary Material available online.

Table 1: Characteristics of the participants included in this study.

Characteristic	PTSD-CI (N=46)	PTSD-CN (N=14)	NPTSD-CI (N=55)	NPTSD-CN (N=63)
Age - Mean (SD)	69.0 (4.0)†	67.9 (2.7)†	73.4 (7.5)	71.3 (5.9)
Years of Education - Mean (SD)	14.3 (2.3)*	14.7 (2.6)*	16.4 (2.3)	16.7 (2.8)
Ethnicity - No (%)				
Not Hispanic/Latino	38 (82.6)†	13 (92.9)	54 (98.2)	61 (96.8)
Hispanic/Latino	7 (15.2)	1 (7.1)	1 (1.8)	2 (3.2)
Unknown	1 (2.2)	0 (0)	0 (0)	0 (0)
Race - No (%)				
Caucasian	38 (82.6)†	14 (100)†	50 (90.9)	55 (87.3)
African American	4 (8.7)	0 (0)	2 (3.6)	6 (9.5)
Asian	0 (0)	0 (0)	2 (3.6)	0 (0)
Mixed	3 (6.5)	0 (0)	1 (1.8)	0 (0)
Indian/Alaskan	1 (2.2)	0 (0)	0 (0)	1 (1.6)
Hawaiian/Other Pacific Islander	0 (0)	0 (0)	0 (0)	0 (0)
Unknown	0 (0)	0 (0)	0 (0)	1 (1.6)
CAPS Current - Mean (SD)	71.8 (22.1)*†	78.8 (13.0)*†	2.9 (5.8)	1.5 (4.8)
MoCA - Mean (SD)	22.1 (2.2)*#	26.8 (1.1)†	22.1 (1.9)*	27.2 (1.1)
ADAS-Cog - Mean (SD)	12.5 (4.2)†	13.8 (2.7)	18.6 (12.4)*	8.7 (4.5)
GDS - Mean (SD)	4.3 (3.3)*†	5.0 (3.3)*†	1.4 (1.2)	0.6 (0.9)
Ecog total - Mean (SD)	1.9 (0.7)*	1.5 (0.4)	2.0 (0.8)*	1.1 (0.2)
MMSE - Mean (SD)	27.9 (1.4)	28.5 (1.1)	26.5 (4.6)*	29.0 (1.1)
CDR - Mean (SD)	0.6 (0.8)*	0.3 (0.4)	2.1 (3.4)*	0.0 (0.2)
ε4 allele - No (%)	21.7†	21.4†	38.2	22.2
Smoking Status - No (%)				
Current Smoker	11.1†	0.0	2.0	7.4
Ever Smoker	73.3*†#	41.7	46.7	49.1
Alcohol Abuse - No (%)	60.0*†	50.0	16.7	14.7

* Indicates a statistically significant difference compared to the NPTSD-CN group.

† Indicates a statistically significant difference compared to the NPTSD-CI group.

 # Indicates a statistically significant difference compared to the PTSD-CN group.

Alcohol abuse within the past 2 years was an exclusion criterion in the ADNI database, while alcohol abuse within the past 5 years was an exclusion criterion in the ADNI-DOD database.

Abbreviations: CAPS, Clinician-Administered PTSD Scale; MoCA, Montreal Cognitive Assessment; ADAS-Cog, Alzheimer's Disease Assessment Scale; GDS, Geriatric Depression Scale; Ecog total, Everyday Cognition scale, total score; MMSE, Mini-Mental State Examination; CDR, Clinical Dementia Rating.

Group differences in whole-brain Florbetapir PET imaging analyses

Compared to NPTSD-CN, amyloid analysis showed significantly increased Florbetapir uptake in the right and left posterofrontal, temporal, and parietal lobes in PTSD-CI patients ($p < 0.001$ uncorrected). This increased tracer binding pattern was not seen in PTSD-CN patients. Qualitatively, PTSD-CI subjects demonstrated overall mildly increased amyloid uptake compared with the NPTSD-CI group versus PTSD-CN subjects. The uptake pattern was also different, with PTSD-CI subjects demonstrating increased amyloid uptake in the bilateral parietal opercular and hippocampal regions, and right greater than left superior temporal gyri (Figure 3). NPTSD-CI showed increased amyloid uptake in the bilateral inferior temporal gyrus and medial parietal lobes (precuneus) as compared to PTSD-CI.
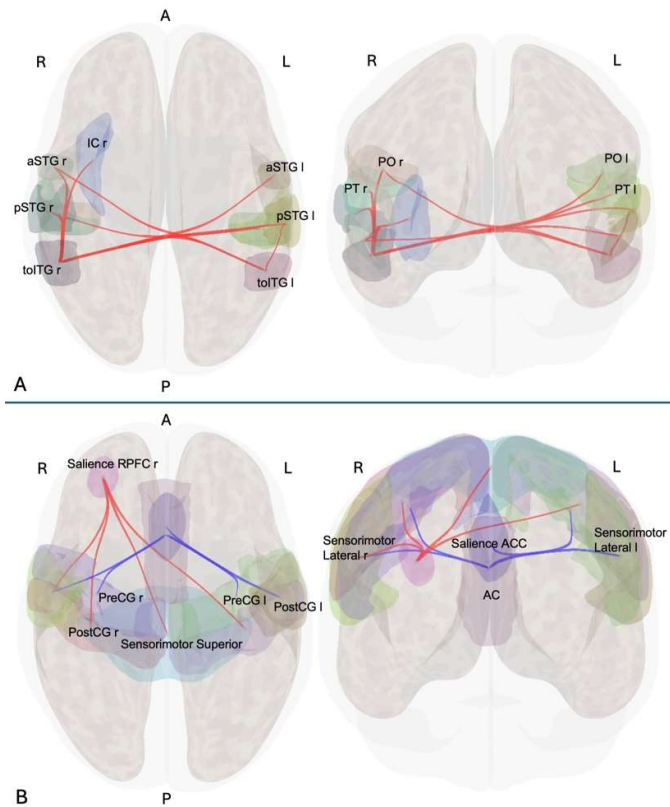
FIG 2. ROI-to-ROI contrast map illustrating nodes with FC increased (red) and decreased FC (blue) for the PTSD-CI (A) and PTSD-CN (B) groups compared to the NPTSD-CN group. Images are displayed in axial (left) and coronal (right) views, with the anterior aspect oriented toward the top and the right side on the right. The ROI-to-ROI connection threshold is set at an uncorrected p-value of < 0.05 (two-sided), and a cluster threshold corrected at p < 0.05 (FDR) (toITG, Inferior Temporal Gyrus, temporooccipital part; PT, Planum Temporale; aSTG l, Superior Temporal Gyrus, anterior division; pSTG, Superior Temporal Gyrus, posterior division; IC, Insular Cortex; PO, Parietal Operculum Cortex; AC, Cingulate Gyrus, anterior division; PreCG, Precentral Gyrus; RPFC, rostral prefrontal cortex; PostCG, Postcentral Gyrus; ACC, anterior cingulate cortex; R, right; L, left, A, anterior; P, posterior).
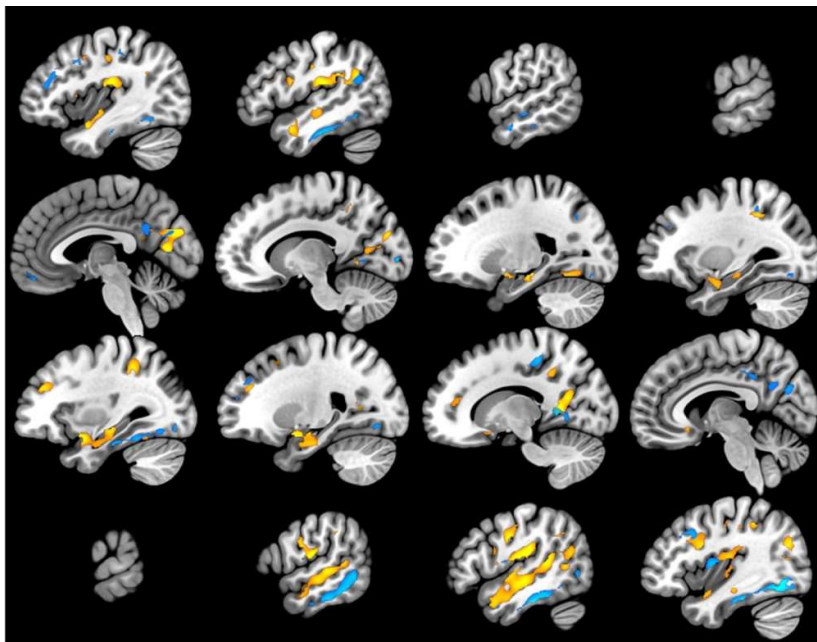

FIG 3. Group differences in Florbetapir PET imaging measures compared to cognitively normal controls (PTSD-CI vs NPTSD-CN; yellow; NPTSD-CI versus NPTSD-CN, blue; p < 0.001 uncorrected, controlling for Age, Education, APOE4 Status, and Depression [GDS] Scores). Images are displayed in the sagittal plane, from farthest left (upper right corner) to farthest right (lower left corner).

Overlapping amyloid PET uptake and FC in PTSD-CI versus NPTSD-CN

Overlapping foci of abnormal amyloid uptake and abnormally increased FC are shown in Figure 4. Dice-Sørensen analysis showed mean overlap between the resting-state fMRI regions of interest and the amyloid thresholded maps (superior temporal gyrus ant and post divisions, right, and bilateral operculum) was 47.9%. The highest overlap was found in the posterior division of the right superior temporal gyrus (56.7%), the left parietal operculum (54.4%), and the right parietal operculum (44.7%). (Table S5).
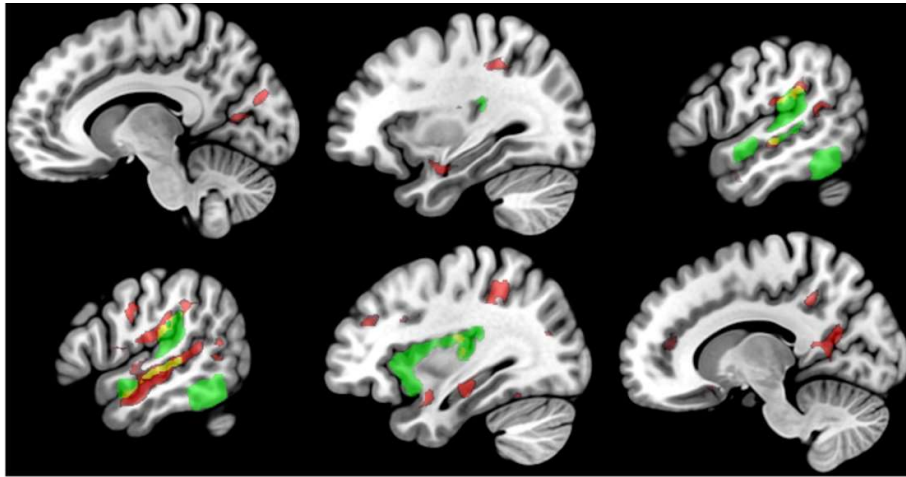

FIG 4. Overlapping amyloid PET uptake and FC in PTSD-CI versus NPTSD-CN. Overlapping foci of abnormal amyloid uptake (red) and abnormally increased FC (green) are seen in the superior temporal gyri, right greater than left, right insula, and bilateral parietal operculum.

DISCUSSION

This study identifies distinct connectivity patterns and amyloid PET uptake in PTSD-CI subjects compared to age-matched controls with or without PTSD or CI. Our choice of resting-state fMRI for connectivity assessment complements the insights from structural imaging techniques like DTI. While DTI is well-suited for evaluating structural connectivity, resting-state fMRI effectively captures dynamic functional interactions, which are particularly relevant for understanding PTSD and its impact on cognitive function. Previous research has demonstrated that rs-fMRI parameters can differentiate amyloid-positive from amyloid-negative individuals, underscoring its sensitivity to early brain activity changes.[12-14] The combination of structural and functional imaging thus offers a broader perspective on the complex neurobiological underpinnings of PTSD.

PTSD-CI subjects, showed significantly increased connectivity between the bilateral temporal lobes and parietal operculum, corresponding with elevated amyloid uptake. Conversely, PTSD-CN subjects exhibited reduced connectivity between the ACC and bilateral somatosensory networks, and increased connectivity between somatosensory networks and the right prefrontal cortex. However, they did not demonstrate an increase in amyloid burden. After adjusting for factors like age, depression scores, APOε4 status, and education, PTSD-CI subjects showed significantly higher amyloid uptake in the inferior parietal lobes (centered in the parietal operculum) and the superior and medial temporal lobes. This pattern slightly contrasts with NPTSD-CI subjects (MOCA scores >18 and <26), who showed greater amyloid uptake in the inferior temporal and precuneus regions. Overlapping regions of increased amyloid uptake and abnormal connectivity, particularly in the parietal operculum and superior temporal gyri, offer potential insights into the mechanisms behind cognitive impairment in PTSD subjects. We propose that this increased connectivity may represent a compensatory response to neuronal dysfunction caused by amyloid deposition. The parietal operculum, a part of the sensorimotor network, is critical for sensory integration and coordination of motor responses.[38] Its heightened activity in PTSD-CI may reflect attempts to maintain sensory and attentional processes in the face of neurodegeneration. Similarly, the superior temporal gyri, implicated in auditory and language processing,[39] may demonstrate increased connectivity to support cognitive functions such as comprehension and memory retrieval. However, we suspect that sustained neuroinflammation and amyloid-mediated toxicity eventually overtakes the compensatory response, leading to an overall decrease in functional connectivity and acceleration in the development of cognitive impairment, as previously shown in Alzheimer's Disease.[12,40]

In our models, the ACC emerged as a critical region in PTSD-CN patients, displaying reduced connectivity with sensorimotor networks bilaterally. In addition, increased connectivity between these sensorimotor regions and the right rostral prefrontal cortex, a part of the salience network, was demonstrated. Changes in the anterior cingulate, amygdala, hippocampus, and insula have been consistently observed across structural and functional MRI studies, supporting the idea that abnormalities in fear learning and threat responses contribute significantly to the development of PTSD.[41]

Moreover, PTSD has been associated with abnormal interactions among the default mode network (DMN) and sensorimotor network, as indicated by a recent meta-analysis of seed-based resting-state functional connectivity studies.[42] The salience network (SN) has also been implicated in PTSD.[43] A systematic review of seed-based functional connectivity studies revealed enhanced SN and decreased DMN connectivity in PTSD. These altered connectivity patterns are thought to reflect increased salience processing and hypervigilance at the expense of internal thought and autobiographical memory in PTSD.[44] However, there remains gaps in the literature concerning resting-

state fMRI studies on PTSD with cognitive decline.

This study suggests that while the anterior insula, sensorimotor, and salience network rostral prefrontal cortex may play a role in PTSD-CN, increased connectivity between the parietal and temporal lobes appears more dominant in PTSD-CI subjects. Resting brain activity in PTSD has been examined,[45] showing significant differences in spontaneous activity in various regions, including the STG, medial prefrontal cortex, inferior parietal lobule, and middle occipital gyrus, as well as limbic areas such as the amygdala, hippocampus, insula, thalamus, and ACC. Yet, results have been inconsistent, often not controlling for cognitive decline or concurrent psychiatric conditions.

The relationship between FC alterations and beta-amyloid depositions in dementia remains debated. Although many studies suggest that declining FC accompanies increased beta-amyloid concentrations, our findings challenge this view. We observed increased amyloid concentrations coincided with regions of increased connectivity between the temporal lobes, particularly the STG, and the parietal and central opercular regions in PTSD-CI subjects. The mean overlap between these resting-state fMRI regions of interest and the amyloid thresholded at $p < 0.001$ (uncorrected) maps using Dice-Sørensen coefficient was 47.9%, with the highest overlap observed in the posterior division of the right superior temporal gyrus (56.7%) and left parietal operculum (54.3%). While this analysis provides a quantifiable measure of overlap, it is important to note that our primary aim is not to evaluate exact correspondence between modalities. Rather, our focus is on the broader distributional patterns, as resting-state fMRI and amyloid PET involve different imaging modalities, thresholds, and analyses. The observed overlap, particularly in the superior temporal gyri and parietal operculum, underscores the convergence of functional and pathological changes in PTSD-CI subjects. This aligns with a meta-analysis on the association between beta-amyloid pathology and FC alterations in Alzheimer's dementia,[46] which found overall positive correlations across 31 studies. The study supports the hypothesis of amyloid-driven transneuronal spreading, which could explain higher FC in regions with more significant protein deposition when global connectivity analysis is applied.[46] Amyloid PET uptake in AD typically occurs in large areas of the neocortex and striatum, sparing the medial temporal lobes. This distribution mirrors postmortem amyloid pathology, with peak uptake seen in the posterior cingulate/precuneus and medial prefrontal regions.[47] However, PTSD-CI subjects displayed a different amyloid deposition pattern, predominantly in the superior and medial temporal lobes, including the hippocampus, the parietal operculum, and the insula. The most significant overlap between FC and amyloid uptake occurred in the superior temporal gyri and parietal operculum. Overall, our findings align with previous research indicating that early beta-amyloid accumulation is associated with increased functional connectivity[15,16], potentially reflecting compensatory mechanisms in response to amyloid deposition in mild cognitive impairment. We suggest that, as seen in Alzheimer's Disease,[12,40] functional connectivity may decrease as the disease progresses to more advanced stages of cognitive decline, which warrants further investigation.

One of the limitations of this study is the small sample size, particularly the PTSD-CN group. However, this group was not our primary focus, since our main interest was the PTSD-CI group. The limited size of the PTSD-CN group stems from the fact that most PTSD subjects in the DOD database exhibited some level of cognitive impairment. It's worth noting that the other groups in our study have sample sizes comparable to or larger than those typically found in systematic reviews and meta-analyses in this field.[44,45] Also, although NPTSD-CI subjects with MOCA scores <18 were excluded, they still scored lower on other cognitive measures. Despite these differences, the PTSD-CI group continued to show increased amyloid distribution relative to NPTSD-CI. Another limitation is the use of subjects from two datasets (ADNI and ADNI-DOD). Subjects in the ADNI-DOD dataset were labeled as controls with regards to their PTSD status alone, leading to subjects labeled as controls by the ADNI-DOD dataset while having an abnormal MOCA score as opposed to our own study, where we labeled controls with regards to both their PTSD and cognitive status. Patients from the ADNI dataset were included to increase our number of control patients. The subjects from the ADNI dataset had an overall higher education level, potentially introducing biases in the results. However, we controlled for education in all our analyses to minimize its potential effect. In addition, our study did not account for medication use. Many benzodiazepine and psychotropic drugs affect resting-state fMRI data.[48,49] While we tried to mitigate this by controlling for depression scores in our analyses (as patients with worse depression symptoms are more likely to take medications), it is unclear how much of an effect the absence of medication data exerts. Finally, while cross-sectional designs, including ours, are commonly employed in neuroimaging studies, they inherently limit our ability to assess how these neuroimaging markers change over time in relation to PTSD and cognitive decline. Longitudinal studies examining imaging biomarkers associated with PTSD to dementia conversion could help stratify individuals at higher risk, enabling targeted preventative interventions.

CONCLUSIONS

In summary, PTSD-CI subjects demonstrate higher amyloid deposition and disruptions in functional connectivity, particularly between the temporal lobes and parietal operculum. The parietal operculum's role in sensory integration and attention and the superior temporal gyri's involvement in language and cognitive control highlight their importance in maintaining cognitive function in PTSD-CI patients. In contrast, PTSD-CN subjects show no increase in amyloid deposition but exhibit abnormal connectivity patterns involving the ACC, sensorimotor cortex, and rostral prefrontal cortex part of the salience network. The relationship between resting-state fMRI connectivity abnormalities and amyloid deposition remains an open question. This study highlights potential mechanisms linking PTSD and CI, supporting previous findings that early beta-amyloid accumulation is associated with increased functional connectivity, possibly reflecting compensatory responses to amyloid deposition. Further research with larger sample sizes and longitudinal data is needed to validate these findings and explore how these changes may influence the progression of cognitive decline.

REFERENCES

1. Prieto S, Nolan KE, Moody JN, Hayes SM, Hayes JP, for the Department of Defense Alzheimer's Disease Neuroimaging I. Posttraumatic stress symptom severity predicts cognitive decline beyond the effect of Alzheimer's disease biomarkers in Veterans. Translational Psychiatry 2023;13(1):102. DOI: 10.1038/s41398-023-02354-0.

2. Clouston SAP, Diminich ED, Kotov R, et al. Incidence of mild cognitive impairment in World Trade Center responders: Long-term consequences of re-experiencing the events on 9/11/2001. Alzheimer's & Dementia: Diagnosis, Assessment & Disease Monitoring 2019;11(1):628-636. DOI: https://doi.org/10.1016/j.dadm.2019.07.006.

3. Yaffe K, Vittinghoff E, Lindquist K, et al. Posttraumatic stress disorder and risk of dementia among US veterans. Arch Gen Psychiatry 2010;67(6):608-13. (In eng). DOI: 10.1001/archgenpsychiatry.2010.61.

4. Günak MM, Billings J, Carratu E, Marchant NL, Favarato G, Orgeta V. Post-traumatic stress disorder as a risk factor for dementia: systematic review and meta-analysis. The British Journal of Psychiatry 2020;217(5):600-608. DOI: 10.1192/bjp.2020.150.

5. Justice NJ, Huang L, Tian J-B, et al. Posttraumatic Stress Disorder-Like Induction Elevates β-Amyloid Levels, Which Directly Activates Corticotropin-Releasing Factor Neurons to Exacerbate Stress Responses. The Journal of Neuroscience 2015;35(6):2612. DOI: 10.1523/JNEUROSCI.3333-14.2015.

6. Carroll JC, Iba M, Bangasser DA, et al. Chronic stress exacerbates tau pathology, neurodegeneration, and cognitive performance through a corticotropin-releasing factor receptor-dependent mechanism in a transgenic mouse model of tauopathy. J Neurosci 2011;31(40):14436-14449.

7. Greenberg MS, Tanev K, Marin MF, Pitman RK. Stress, PTSD, and dementia. Alzheimer's & Dementia 2014;10:S155-S165.

8. Alves de Araujo Junior D, Sair HI, Peters ME, et al. The association between post-traumatic stress disorder (PTSD) and cognitive impairment: A systematic review of neuroimaging findings. J Psychiatr Res 2023;164:259-269. (In eng). DOI: 10.1016/j.jpsychires.2023.06.016.

9. Viviano RP, Damoiseaux JS. Functional neuroimaging in subjective cognitive decline: current status and a research path forward. Alzheimers Res Ther 2020;12(1):23. DOI: 10.1186/s13195-020-00591-9.

10. Akiki TJ, Averill CL, Wrocklage KM, et al. Default mode network abnormalities in posttraumatic stress disorder: A novel network-restricted topology approach. Neuroimage 2018;176:489-498. DOI: 10.1016/j.neuroimage.2018.05.005.

11. Wang SM, Kim NY, Kang DW, et al. A Comparative Study on the Predictive Value of Different Resting-State Functional Magnetic Resonance Imaging Parameters in Preclinical Alzheimer's Disease. Front Psychiatry 2021;12:626332. DOI: 10.3389/fpsyt.2021.626332.

12. Han F, Liu X, Mailman RB, Huang X, Liu X. Resting-state global brain activity affects early beta-amyloid accumulation in default mode network. Nat Commun 2023;14(1):7788. DOI: 10.1038/s41467-023-43627-y.

13. Michels L, Muthuraman M, Anwar AR, et al. Changes of Functional and Directed Resting-State Connectivity Are Associated with Neuronal Oscillations, ApoE Genotype and Amyloid Deposition in Mild Cognitive Impairment. Front Aging Neurosci 2017;9:304. DOI: 10.3389/fnagi.2017.00304.

14. Sheline YI, Raichle ME. Resting state functional connectivity in preclinical Alzheimer's disease. Biol Psychiatry 2013;74(5):340-7. DOI: 10.1016/j.biopsych.2012.11.028.

15. Song Z, Insel PS, Buckley S, et al. Brain amyloid-beta burden is associated with disruption of intrinsic functional connectivity within the medial temporal lobe in cognitively normal elderly. J Neurosci 2015;35(7):3240-7. DOI: 10.1523/JNEUROSCI.2092-14.2015.

16. Hahn A, Strandberg TO, Stomrud E, et al. Association Between Earliest Amyloid Uptake and Functional Connectivity in Cognitively Unimpaired Elderly. Cereb Cortex 2019;29(5):2173-2182. DOI: 10.1093/cercor/bhz020.

17. Munro CE, Farrell M, Hanseeuw B, et al. Change in Depressive Symptoms and Longitudinal Regional Amyloid Accumulation in Unimpaired Older Adults. JAMA Netw Open 2024;7(8):e2427248-e2427248. DOI: 10.1001/jamanetworkopen.2024.27248.

18. Javaheripour N, Li M, Chand T, et al. Altered resting-state functional connectome in major depressive disorder: a mega-analysis from the PsyMRI consortium. Translational Psychiatry 2021;11(1):511. DOI: 10.1038/s41398-021-01619-w.

19. Mulders PC, van Eijndhoven PF, Schene AH, Beckmann CF, Tendolkar I. Resting-state functional connectivity in major depressive disorder: A review. Neuroscience & Biobehavioral Reviews 2015;56:330-344. DOI: https://doi.org/10.1016/j.neubiorev.2015.07.014.

20. Iraji A, Benson RR, Welch RD, et al. Resting State Functional Connectivity in Mild Traumatic Brain Injury at the Acute Stage: Independent Component and Seed-Based Analyses. J Neurotrauma 2015;32(14):1031-45. (In eng). DOI: 10.1089/neu.2014.3610.

21. Bickart K, Sheridan C, Frees D, et al. A Systematic Review of Resting-State fMRI in Traumatic Brain Injury Across Injury Age, Severity, Mechanism, Chronicity, and Imaging Methods (P8-1.009). Neurology 2023;100(17_supplement_2):4146. DOI: 10.1212/WNL.0000000000203779.

22. Malkki H. PET imaging detects amyloid deposits after TBI. Nature Reviews Neurology 2014;10(1):3-3. DOI: 10.1038/nrneurol.2013.250.

23. Mohamed AZ, Cumming P, Srour H, et al. Amyloid pathology fingerprint differentiates post-traumatic stress disorder and traumatic brain injury. Neuroimage Clin 2018;19:716-726. (In eng). DOI: 10.1016/j.nicl.2018.05.016.

24. Weiner MW, Harvey D, Landau SM, et al. Traumatic brain injury and post-traumatic stress disorder are not associated with Alzheimer's disease pathology measured with biomarkers. Alzheimer's & Dementia 2023;19(3):884-895. DOI: https://doi.org/10.1002/alz.12712.

25. Hagger-Johnson G, Sabia S, Brunner EJ, et al. Combined impact of smoking and heavy alcohol use on cognitive decline in early old age: Whitehall II prospective cohort study. Br J Psychiatry 2013;203(2):120-5. DOI: 10.1192/bjp.bp.112.122960.

26. Mast BT, Gerstenecker A. Chapter 19 - Screening Instruments and Brief Batteries for Dementia. In: Lichtenberg PA, ed. Handbook of Assessment in Clinical Gerontology (Second Edition). San Diego: Academic Press; 2010:503-530.

27. Elias A, Cummins T, Lamb F, et al. Amyloid-β, Tau, and 18F-Fluorodeoxyglucose Positron Emission Tomography in Posttraumatic Stress Disorder. J Alzheimers Dis 2020;73(1):163-173. (In eng). DOI: 10.3233/jad-190913.

28. Nasreddine ZS, Phillips NA, Bedirian V, et al. The Montreal Cognitive Assessment, MoCA: a brief screening tool for mild cognitive impairment. J Am Geriatr Soc 2005;53(4):695-9. DOI: 10.1111/j.1532-5415.2005.53221.x.

29. Jack CR, Jr., Bernstein MA, Borowski BJ, et al. Update on the magnetic resonance imaging core of the Alzheimer's disease neuroimaging initiative. Alzheimers Dement 2010;6(3):212-20. (In eng). DOI: 10.1016/j.jalz.2010.03.004.

30. Whitfield-Gabrieli S, Nieto-Castanon A. Conn: a functional connectivity toolbox for correlated and anticorrelated brain networks. Brain Connect 2012;2(3):125-41. DOI: 10.1089/brain.2012.0073.

31. Nieto-Castanon A, Whitfield-Gabrieli S. CONN functional connectivity toolbox: RRID SCR_009550, release 20: Hilbert Press, 2020.

32. Ashburner J, Friston KJ. Unified segmentation. NeuroImage 2005;26(3):839-851. DOI: https://doi.org/10.1016/j.neuroimage.2005.02.018.

33. Penny WD, Friston KJ, Ashburner JT, Kiebel SJ, Nichols TE. Statistical parametric mapping: the analysis of functional brain images: Elsevier, 2011.

34. Desikan RS, Segonne F, Fischl B, et al. An automated labeling system for subdividing the human cerebral cortex on MRI scans into gyral based regions of interest. Neuroimage 2006;31(3):968-80. DOI: 10.1016/j.neuroimage.2006.01.021.

35. Jenkinson M, Beckmann CF, Behrens TEJ, Woolrich MW, Smith SM. FSL. NeuroImage 2012;62(2):782-790. DOI: 10.1016/j.neuroimage.2011.09.015.

36. Cohen AD, Price JC, Weissfeld LA, et al. Basal cerebral metabolism may modulate the cognitive effects of Abeta in mild cognitive impairment: an example of brain reserve. J Neurosci 2009;29(47):14770-8. DOI: 10.1523/JNEUROSCI.3669-09.2009.

37. Zou KH, Warfield SK, Bharatha A, et al. Statistical validation of image segmentation quality based on a spatial overlap index. Acad Radiol 2004;11(2):178-89. DOI: 10.1016/s1076-6332(03)00671-8.

38. Sirigu A, Desmurget M. Somatosensory awareness in the parietal operculum. Brain 2021;144(12):3558-3560. DOI: 10.1093/brain/awab415.

39. Yi HG, Leonard MK, Chang EF. The Encoding of Speech Sounds in the Superior Temporal Gyrus. Neuron 2019;102(6):1096-1110. DOI: 10.1016/j.neuron.2019.04.023.

40. Ingala S, Tomassen J, Collij LE, et al. Amyloid-driven disruption of default mode network connectivity in cognitively healthy individuals. Brain Commun 2021;3(4):fcab201. DOI: 10.1093/braincomms/fcab201.

41. Kunimatsu A, Yasaka K, Akai H, Kunimatsu N, Abe O. MRI findings in posttraumatic stress disorder. Journal of Magnetic Resonance Imaging 2020;52(2):380-396. DOI: https://doi.org/10.1002/jmri.26929.

42. Bao W, Gao Y, Cao L, et al. Alterations in large-scale functional networks in adult posttraumatic stress disorder: A systematic review and meta-analysis of resting-state functional connectivity studies. Neuroscience & Biobehavioral Reviews 2021;131:1027-1036. DOI: https://doi.org/10.1016/j.neubiorev.2021.10.017.

43. Abdallah CG, Averill CL, Ramage AE, et al. Salience Network Disruption in U.S. Army Soldiers With Posttraumatic Stress Disorder. Chronic Stress 2019;3:2470547019850467. DOI: 10.1177/2470547019850467.

44. Koch SBJ, van Zuiden M, Nawijn L, Frijling JL, Veltman DJ, Olff M. ABERRANT RESTING-STATE BRAIN ACTIVITY IN POSTTRAUMATIC STRESS DISORDER: A META-ANALYSIS AND SYSTEMATIC REVIEW. Depression and Anxiety 2016;33(7):592-605. DOI: https://doi.org/10.1002/da.22478.

45. Wang T, Liu J, Zhang J, et al. Altered resting-state functional activity in posttraumatic stress disorder: A quantitative meta-analysis. Scientific Reports 2016;6(1):27131. DOI: 10.1038/srep27131.

46. Hasani Seyede A, Mayeli M, Salehi Mohammad A, Barzegar Parizi R. A Systematic Review of the Association between Amyloid-β and τ Pathology with Functional Connectivity Alterations in the Alzheimer Dementia Spectrum Utilizing PET Scan and rsfMRI. Dementia and Geriatric Cognitive Disorders Extra 2021;11(2):78-90. DOI: 10.1159/000516164.

47. Chapleau M, Iaccarino L, Soleimani-Meigooni D, Rabinovici GD. The Role of Amyloid PET in Imaging Neurodegenerative Disorders: A Review. Journal of Nuclear Medicine 2022;63(Supplement 1):13S. DOI: 10.2967/jnumed.121.263195.

48. Wandschneider B, Koepp MJ. Pharmaco fMRI: Determining the functional anatomy of the effects of medication. Neuroimage

Clin 2016;12:691-697. DOI: 10.1016/j.nicl.2016.10.002.

49.   Hafeman DM, Chang KD, Garrett AS, Sanders EM, Phillips ML. Effects of medication on neuroimaging findings in bipolar disorder: an updated review. Bipolar Disord 2012;14(4):375-410. DOI: 10.1111/j.1399-5618.2012.01023.x.

SUPPLEMENTAL FILES

Materials and Methods

rs-fMRI data preprocessing

Preprocessing steps included motion correction, slice timing correction, and ART-based outlier detection (https://www.nitrc.org/projects/artifact_detect/).[25] Original voxel size was 3.4 x 3.4 x 3.4 mm³. Data were normalized to the MNI152 template space with a $2 \times 2 \times 2$ mm³ resampling voxel size and spatially smoothed using an 8 mm FWHM Gaussian kernel. T1-weighted MPRAGE structural scans were also normalized and segmented into grey matter, white matter, and cerebrospinal fluid (CSF). Denoising followed the standard pipeline,[22] with linear detrending and regression of confounding variables, including WM and CSF signals (5 CompCor components each), realignment parameters (12 parameters), and scrubbing variables. A band-pass filter (0.01–0.1 Hz) was applied to minimize physiological and motion-related noise.

1.2.   PET data preprocessing

All PET images of each subject were registered to their T1-weighted images using the FMRIB Linear Image Registration Tool (FLIRT; http://www.fmrib.ox.ac. uk/fsl/fslwiki/FLIRT).[28] The T1-weighted images were spatially normalized to the Montreal Neurological Institute (MNI)-152 template and the transformation parameters were subsequently applied to warp the PET images to the MNI space. Afterward, the PET data were quantified using the standard uptake value ratio (SUVR) referenced by the mean uptake in the whole cerebellum and smoothed with an 8 mm FWHM Gaussian kernel. All images were checked for the presence of nonperfect fits before analysis.

Methods

Group differences in whole-brain ROI-to-ROI rs-fMRI imaging analyses

PTSD-CI vs PTSD-CN

No significant connectivity changes at the cluster level were observed when comparing PTSD-CI and PTSD-CN patients. However, at the ROI level (cluster threshold: p < 0.05, ROI-level FDR corrected; connection threshold: uncorrected p < 0.01), several regions showed increased connectivity with the anterior insula in PTSD-CI patients compared to PTSD-CN (Figure S1A). Additionally, decreased connectivity was noted between the cerebellum and anterior insula (Table S3).

PTSD-CI vs NPTSD-CI

A cluster comprising 11 ROIs and 28 statistically positive connections among them was observed involving the subcallosal cortex (SubCalC) and bilateral basal ganglia, thalami and nucleus accumbens (Figure S1B and Table S4).
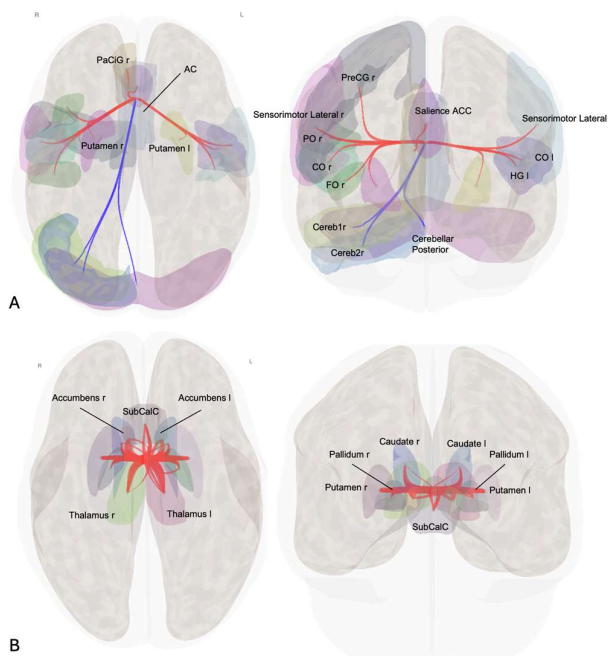

FIG S1. ROI-to-ROI contrast map illustrating nodes with FC (red) and decreased FC (blue) for the PTSD-CI compared to the PTSD-CN group (A) and PTSD-CI compared to NPTSD-CI group (B). Images are displayed in axial and coronal views, with the anterior aspect oriented toward the top and the right side on the right. In A, the network-defining threshold (connection-wise) was set to

p < 0.01, and the ROI-level results were FDR-corrected for multiple comparisons (p < 0.05) at the ROI level. In B, the connection threshold is set at an uncorrected p-value of < 0.05 and the cluster threshold FDR-corrected at p < 0.05 (ACC, anterior cingulate cortex; PreCG, precentral gyrus; AC, Cingulate Gyrus, anterior division; PaCiG, paracingulate gyrus; PO, parietal operculum; CO, central opercular cortex; FO, frontal operculum; Cerebe1r, cerebellum crus1; Cereb2r, cerebellum crus2; HG, Heschl's gyrus; SubcalC, subcallosal cortex; r, right; l, left).

Table S1. Whole-brain ROI-to-ROI Analysis Comparing PTSD-CI and NPTSD-CN Groups, Controlling for Age, Education, APOE4 Status, and Depression (GDS) Scores (cluster threshold corrected at p < 0.05 [FDR]).

		Beta value	T Statistic	p-uncorrected	p-FDR
Cluster			7.97	0.000007	0.002277
Superior Temporal Gyrus, posterior division Left	Inferior Temporal Gyrus, temporooccipital part Right	0.23	4.97	0.000002	0.000277
Superior Temporal Gyrus, posterior division Left	Inferior Temporal Gyrus, temporooccipital part Left	0.13	3.25	0.001393	0.077063
Superior Temporal Gyrus, anterior division Right	Inferior Temporal Gyrus, temporooccipital part Right	0.13	2.72	0.007346	0.089568
Planum Temporale Left	Inferior Temporal Gyrus, temporooccipital part Right	0.16	3.43	0.000769	0.127672
Planum Temporale Right	Inferior Temporal Gyrus, temporooccipital part Right	0.13	2.80	0.005772	0.198223
Superior Temporal Gyrus, anterior division Left	Inferior Temporal Gyrus, temporooccipital part Right	0.14	3.26	0.001352	0.224506
Superior Temporal Gyrus, anterior division Right	Inferior Temporal Gyrus, temporooccipital part Left	0.085	1.98	0.049148	0.254956
Superior Temporal Gyrus, posterior division Right	Inferior Temporal Gyrus, temporooccipital part Right	0.12	2.67	0.008418	0.635499
Parietal Operculum Cortex Right	Inferior Temporal Gyrus, temporooccipital part Right	0.12	2.44	0.0158	0.681922
Parietal Operculum Cortex Right	Inferior Temporal Gyrus, temporooccipital part Left	0.12	2.42	0.016432	0.681922
Insular Cortex Right	Inferior Temporal Gyrus, temporooccipital part Right	0.099	2.01	0.046553	0.754147
Parietal Operculum Cortex Left	Inferior Temporal Gyrus, temporooccipital part Right	0.12	2.44	0.015714	0.99978

Table S2. Whole-brain ROI-to-ROI Analysis Comparing PTSD-NCI and NPTSD-CN Groups, Controlling for Age, Education, APOE4 Status, and Depression (GDS) Scores (cluster threshold corrected at p < 0.05 [FDR]).

		Beta value	T Statistic	p-uncorrected	p-FDR
Cluster			7.34	0.00019	0.006111
SensoriMotor.Lateral Left (-55,-12,29)	Cingulate Gyrus, anterior division	0.19	-3.78	0.000219	0.03635
Precentral Gyrus Left	Cingulate Gyrus, anterior division	0.16	-3.35	0.000991	0.082226
SensoriMotor Lateral Right (56,-10,29)	Cingulate Gyrus, anterior division	0.2	-3.44	0.000739	0.122742
SensoriMotor Superior (0,-31,67)	Salience RPFC Right (32,46,27)	-0.031	3.19	0.001725	0.286425
Precentral Gyrus Right	Cingulate Gyrus, anterior division	0.18	-2.55	0.01169	0.323429
Postcentral Gyrus Right	Salience RPFC Right (32,46,27)	-0.05	2.90	0.004214	0.349744
SensoriMotor Lateral Right (56,-10,29)	Salience RPFC Right (32,46,27)	0.016	2.14	0.03417	0.535989
SensoriMotor Lateral Left (-55,-12,29)	Salience ACC (0,22,35)	0.16	-2.59	0.010416	0.576356
Postcentral Gyrus Left	Salience RPFC Right (32,46,27)	-0.062	2.49	0.013828	0.689052

RPFC= rostral prefrontal cortex; ACC = anterior cingulate cortex

Table S3. Whole-brain ROI-to-ROI Analysis Comparing PTSD-CI and PTSD-CN Groups.

ROI-level connections		Beta value	T Statistic	p-uncorrected	p-FDR
Cingulate Gyrus, anterior division	Cerebellum Crus1 Right	-0.24	-4.35	0.000056	0.009311
	Central Opercular Cortex Left	0.15	3.88	0.000266	0.022117
	Putamen Right	0.17	3.67	0.000522	0.028902
	Central Opercular Cortex Right	0.18	3.46	0.001017	0.042214
	SensoriMotor Lateral Right (56,-10,29)	0.16	3.38	0.001285	0.042672
	Cerebellar Posterior (0,-79,-32)	-0.22	-3.26	0.001869	0.042973
	Putamen Left	0.14	3.23	0.002014	0.042973
	Frontal Operculum Cortex Right	0.26	3.18	0.002343	0.042973
	Parietal Operculum Cortex Right	0.2	3.17	0.002459	0.042973
	SensoriMotor Lateral Left (-55,-12,29)	0.13	3.15	0.002589	0.042973
	Heschl's Gyrus Left	0.11	3.08	0.003154	0.044343
	Cerebellum Crus2 Right	-0.18	-3.08	0.003206	0.044343
	Paracingulate Gyrus Right	0.67	2.91	0.005114	0.060891
	Salience ACC (0,22,35)	0.96	2.91	0.005135	0.060891
	Precentral Gyrus Right	0.16	2.84	0.006207	0.068696

ACC = anterior cingulate cortex

Table S4. Whole-brain ROI-to-ROI Analysis Comparing PTSD-CI and NPTSD-CI Groups, Controlling for Age, Education, APOE4 Status, and Depression (GDS) Scores.

Cluster-level connections		Beta value	T Statistic	p-uncorrected	p-FDR
Thalamus r	Thalamus l	1.14	4.36	0.000023	0.003805
Caudate r	Caudate l	0.956	3.88	0.000149	0.024787
Putamen l	Putamen r	0.881	3.73	0.000268	0.04448
Accumbens l	Thalamus r	0.213	3.20	0.001664	0.045785
Subcallosal Cortex	Accumbens l	0.285	3.61	0.000415	0.046964
Accumbens l	Thalamus l	0.227	2.63	0.009395	0.086641
Subcallosal Cortex	Accumbens r	0.289	3.14	0.002014	0.111466
Accumbens l	Putamen r	0.281	2.37	0.019147	0.132435
Accumbens r	Putamen r	0.235	3.20	0.001667	0.167198
Thalamus l	Putamen l	0.287	2.95	0.003647	0.195492
Caudate l	Putamen r	0.258	2.77	0.006214	0.200387
Caudate l	Putamen l	0.267	2.76	0.00637	0.200387
Thalamus l	Putamen r	0.244	2.78	0.006089	0.202143
Pallidum l	Pallidum r	0.441	2.87	0.004726	0.280536
Thalamus r	Caudate l	0.318	2.08	0.03874	0.370683
Thalamus r	Putamen r	0.252	2.04	0.043246	0.370683
Pallidum l	Thalamus l	0.195	2.31	0.022019	0.377209
Pallidum l	Thalamus r	0.155	2.22	0.028107	0.393954
Pallidum l	Putamen l	0.339	2.13	0.034548	0.393954
Subcallosal Cortex	Caudate r	0.153	2.07	0.040099	0.422139
Pallidum r	Putamen l	0.241	2.83	0.005252	0.435892
Caudate r	Putamen l	0.211	2.49	0.013766	0.43739
Caudate r	Putamen r	0.215	2.31	0.02234	0.444316
Accumbens r	Accumbens l	0.59	2.32	0.02153	0.661046
Accumbens r	Caudate l	0.313	2.30	0.022758	0.661046
Accumbens r	Putamen l	0.254	2.23	0.027216	0.661046
Accumbens r	Thalamus l	0.238	2.10	0.037636	0.690056
Pallidum r	Thalamus l	0.175	2.15	0.032784	0.792705

r = Right; l = Left

Table S5. Dice-Sørensen analysis of the overlap between the resting-state fMRI regions of interest and the amyloid thresholded maps.

Region	Percent overlap (%)
Right superior temporal gyrus, anterior division	35.9
Left superior temporal gyrus, anterior division	3.6
Right superior temporal gyrus, posterior division	56.7
Left superior temporal gyrus, posterior division	8.4
Right planum temporale	2.9
Left planum temporale	0.1
Right parietal operculum cortex	44.7
Left parietal operculum cortex	54.4
Right insular cortex	16.1
Right inferior temporal gyrus, temporooccipital part	0
Left inferior temporal gyrus, temporooccipital part	0